

A Brief History of Timing

N. Cartiglia^{a,*}

^a*INFN sezione di Torino, Torino, Italy*

Abstract

This review traces the evolution of precision timing in particle physics experiments, from the first large-scale applications of scintillator and photomultiplier tube (PMT) systems in the 1990s to the picosecond-precision detectors of future colliders. Four technological generations are identified: (i) the era of discrete electronics (NIM, CAMAC, VME) and PMTs, which established the three canonical uses of timing – particle identification via time-of-flight, background and pile-up rejection, and directionality triggering; (ii) the silicon revolution enabled by Silicon Photomultipliers (SiPMs), Low-Gain Avalanche Diodes (LGADs), and Application-Specific Integrated Circuits (ASICs); (iii) the current transition to ubiquitous four-dimensional (4D) tracking, in which time is a coordinate measured at every point along a particle trajectory. Under-construction systems at the HL-LHC (CMS MTD, ATLAS HGTD, CMS HGCAL) demonstrate the maturity of 30–50 ps silicon timing at the million-channel scale. The EIC, LHCb VELO Upgrade II, and ALICE 3 push this technology into new regimes of radiation hardness, material budget, and granularity. (iv) The Far-future facilities such as the Muon Collider and FCC require a further leap to ~10 ps, setting the agenda for the next decade of detector R&D.

Keywords: timing detectors, LGAD, SiPM, 4D tracking, time-of-flight, pile-up rejection, CMS MTD, ATLAS HGTD, LHCb, EIC, FCC, Muon Collider

Contents

| | | |
|----------|--|----------|
| 1 | Introduction | 2 |
| 2 | Timing Technologies 1990s–2010s | 3 |
| 2.1 | Physics motivations | 3 |
| 2.2 | PMTs - Scintillators systems | 4 |
| 2.3 | Water Cherenkov detectors: the Kamiokande legacy | 4 |
| 2.4 | The MRPC family: gaseous timing | 5 |
| 2.5 | The Cherenkov family: DIRC and TOP | 6 |
| 3 | The Silicon Revolution | 7 |
| 3.1 | Silicon Photomultiplier (SiPM) | 7 |
| 3.2 | Low-Gain Avalanche Diode (LGAD / UFSD) | 8 |
| 3.3 | Resistive Silicon Detector (RSD / AC-LGAD) | 10 |

*Corresponding author

Email address: cartiglia@to.infn.it (N. Cartiglia)

| | | |
|-----------|---|-----------|
| 4 | From 3+1 to 4D Tracking | 11 |
| 4.1 | The conceptual shift | 11 |
| 4.2 | The 4D tracking challenge | 11 |
| 5 | Timing Systems Under Construction | 12 |
| 5.1 | CMS MIP Timing Detector (MTD) | 12 |
| 5.2 | ATLAS High-Granularity Timing Detector (HGTD) | 13 |
| 5.3 | CMS High-Granularity Calorimeter (HGCAL) | 13 |
| 6 | Timing in New and Near-Future Experiments | 14 |
| 6.1 | PIONEER at PSI | 14 |
| 6.2 | Electron-Ion Collider (EIC / ePIC) | 14 |
| 6.3 | LHCb VELO Upgrade II: the first 4D vertex detector | 14 |
| 6.4 | ALICE 3 | 15 |
| 7 | Timing in Far-Future Experiments | 15 |
| 7.1 | FCC-ee | 15 |
| 7.2 | Muon Collider | 16 |
| 7.3 | FCC-hh | 16 |
| 8 | Timing in future Calorimeters | 16 |
| 8.1 | LHCb PicoCal | 16 |
| 8.2 | Crilin for the Muon Collider | 17 |
| 8.3 | Dual-readout calorimetry: IDEA / FCC-ee | 17 |
| 9 | Timing in future Gaseous and Cherenkov detectors | 17 |
| 9.1 | TORCH at LHCb Upgrade II | 18 |
| 9.2 | PICOSEC Micromegas | 18 |
| 9.3 | 4D-RICH | 18 |
| 10 | Timing in future Satellite Experiments | 18 |
| 11 | Timing ASICs | 19 |
| 11.1 | The NA62 GigaTracker | 19 |
| 11.2 | ASICs for the ATLAS and CMS timing layers at the HL-LHC | 19 |
| 11.3 | ASICs for EIC | 20 |
| 11.4 | Next-generation frontier: 28 nm ASICs | 20 |
| 11.5 | Alternative paths: waveform digitizers | 21 |
| 12 | Future Challenges | 21 |
| 13 | Conclusions | 22 |

1. Introduction

Timing has always been a tool in high-energy physics experiments, but its role has changed qualitatively over the past three decades. In the 1990s, a dedicated timing system measured the transit time of a particle between two scintillating planes: a single number per track, used offline

for particle identification or event selection. Today, experiments under construction read out millions of silicon pixels, each providing both a position and a time-stamp with a precision of 25–50 ps, and future facilities aim for a factor of five improvement on this figure.

This transformation was driven by two converging pressures. On the physics side, the luminosity frontier has produced collision pile-up densities that can no longer be resolved by spatial tracking alone; at the HL-LHC an average of 200 proton–proton interactions occur per bunch crossing, yielding to overlapping interactions along the beam axis but distributed over a time interval of about ~ 150 ps. A time-stamp at the track level with a resolution of ~ 50 ps allows the reconstruction algorithms to assign tracks to primary vertices with high fidelity. On the technology side, three inventions removed the obstacles that had prevented the integration of fast timing at the pixel level: the Silicon Photomultiplier (SiPM), the Low-Gain Avalanche Diode (LGAD), and ASIC able to measure timing with high resolution (timing ASICs).

The structure of this review follows the historical arc of these developments. Section 2 covers the era of PMT-based systems and their three canonical physics applications. Section 3 describes the silicon revolution and its enabling technologies. Section 4 discusses the conceptual shift from a dedicated timing layer to full 4D tracking. Sections 5–7 survey the landscape of systems under construction and planned for future facilities, organised by experiment and era. Section 11 reviews the corresponding ASIC development. Sections 8–9 cover timing in calorimetry and gaseous/Cherenkov detectors. Section 10 addresses the particular constraints of space-borne experiments. Section 12 outlines open challenges, and Section 13 concludes.

2. Timing Technologies 1990s–2010s

2.1. Physics motivations

Before the advent of silicon timing detectors, nearly all timing applications in particle physics relied on three components: a scintillator pad or bar, a photomultiplier tube (PMT), and a chain of discrete electronics in NIM, CAMAC, or VME crates. A Minimum Ionising Particle (MIP) traversing the scintillator deposits energy that is converted to a burst of optical photons; these are converted to an electrical pulse by the PMT, which is then digitised and time-stamped by the downstream electronics. Systems of this type typically achieved time resolutions of 100–200 ps, occupied volumes of 1–25 m², and required a few hundred PMTs operating at 1–2 kV.

These systems were deployed for three distinct physics goals, illustrated schematically in Fig. 1:

Particle Identification (PID) via Time-of-Flight (TOF). By measuring the transit time of a particle between two detectors separated by a known distance L , one can determine its velocity $\beta = L/(ct)$. Combined with the momentum p measured by a magnetic spectrometer, the mass $m^2 = p^2(1/\beta^2 - 1)$ discriminates between pion, kaon, and proton hypotheses. For typical momenta of 1–3 GeV/ c and flight paths of 1–2 m, a resolution of 100 ps provides 3σ π/K separation up to ~ 1.5 GeV/ c .

Pile-up and background rejection. In fixed-target and collider experiments with high beam rates, timing resolves overlapping events in time and suppresses accidental coincidences. A sub-nanosecond window around the beam bunch eliminates out-of-time activity from halo particles, photons converted upstream, or interactions of secondary beams.

Directionality and triggering. The relative arrival times of signals in different detector layers determine whether a particle is travelling upward or downward, an essential tool for separating cosmic-ray albedo from genuine upward-going neutrino-induced muons in underground and space-borne detectors.

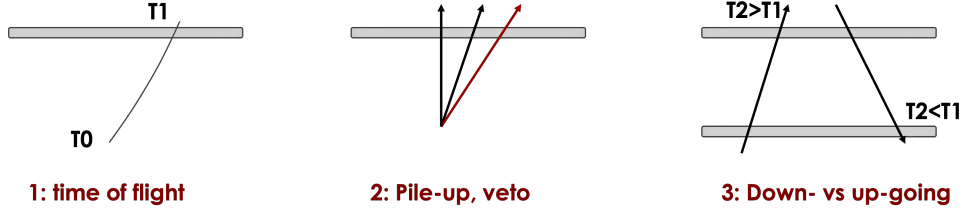


Figure 1: The three canonical uses of timing in particle physics. (1) *Time-of-flight*: a particle traverses a known distance between a start counter (T0) and a stop counter (T1); the transit time determines its velocity and, combined with momentum, its mass. (2) *Pile-up and veto*: multiple particles arrive at the same detector at different times; the out-of-time track (red) is rejected by a timing window. (3) *Directionality*: two stacked detectors measure T_1 and T_2 ; a downward-going particle satisfies $T_2 > T_1$, while an upward-going particle satisfies $T_2 < T_1$.

2.2. PMTs - Scintillators systems

CDF-II Time-of-Flight. The CDF-II detector at the Tevatron added a TOF barrel system between the central outer tracker and the solenoid (Fig. 2, left) [1]. It comprised 216 scintillator bars of dimension $3 \times 3 \times 279 \text{ cm}^3$, read out by fine-mesh PMTs capable of operating in the 1.4 T solenoidal field. The system achieved a time resolution of $\sim 100 \text{ ps}$ and provided $1.5 \sigma K/\pi$ separation at $1.6 \text{ GeV}/c$, improving the charged-kaon tagging efficiency for B -meson flavour identification by approximately 20%.

NA48 and KTeV. The NA48 experiment at CERN measured direct CP violation in $K_L \rightarrow \pi\pi$ decays by comparing simultaneous K_L and K_S beams [2]. The Liquid Krypton (LKr) electromagnetic calorimeter provided intrinsic timing at the $\sim 300 \text{ ps}$ level, supplemented by a plastic-scintillator hodoscope with $\sim 150 \text{ ps}$ resolution. Timing was essential to reject accidental associations between the two beams and to define the fiducial decay volume. KTeV at Fermilab employed a similar strategy with a CsI calorimeter [3].

AMS-02. The Alpha Magnetic Spectrometer on the International Space Station uses four layers of plastic-scintillator TOF paddles, read out by PMTs (Fig. 2, right) [4]. The system achieves $\sim 160 \text{ ps}$ time resolution and serves three roles simultaneously: primary trigger generation for the magnetic spectrometer, charge measurement via dE/dx , and up/down discrimination to separate cosmic-ray albedo protons from genuine upward-going particles. Notably, AMS-02 already used custom ASICs in parts of its readout chain, an early example of the integration trend that would later define silicon timing systems.

2.3. Water Cherenkov detectors: the Kamiokande legacy

Water Cherenkov detectors represent a distinct class in which timing is not an auxiliary measurement but the *primary reconstruction tool*. In experiments such as Kamiokande and its successors Super-Kamiokande and Hyper-Kamiokande [5] (Fig. 3), the position of a neutrino interaction vertex and the direction of the resulting charged lepton are reconstructed entirely from the

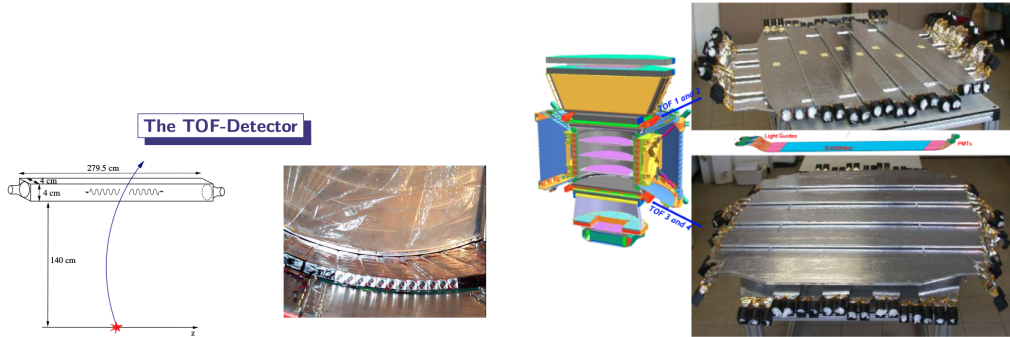


Figure 2: Left: The CDF-II Time-of-Flight detector, showing the cylindrical arrangement of scintillator bars (length 279.5 cm) and fine-mesh PMTs at both ends, positioned between the outer tracking volume and the solenoid at a radius of 140 cm [1]. Right: One of the four AMS-02 TOF planes, illustrating the scintillator paddles with light guides and PMTs.

relative arrival times of Cherenkov photons at the surrounding wall of PMTs. A photon travelling at speed c from a vertex at position \vec{r}_0 arrives at PMT i at time $t_i = |\vec{r}_i - \vec{r}_0|/c + t_0$. A fit over all PMTs with at least one detected photon determines \vec{r}_0 and t_0 with a spatial precision of ~ 30 cm for sub-GeV events. The precision of this reconstruction depends directly on the single-photon transit-time spread of the PMTs, which in Super-Kamiokande is ~ 2 ns for 50-cm diameter tubes, and on the coverage fraction.

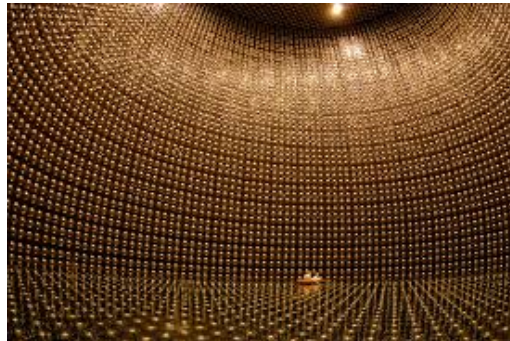


Figure 3: Interior of the Super-Kamiokande detector, showing the array of 50 cm diameter PMTs covering the cylindrical walls, floor, and ceiling of the 50 kt water volume. Vertex and direction reconstruction rely entirely on the relative arrival times of Cherenkov photons across the PMT array, making Super-Kamiokande one of the earliest examples of timing as the primary reconstruction tool rather than an auxiliary measurement [5].

2.4. The MRPC family: gaseous timing

The Multigap Resistive Plate Chamber (MRPC) was developed in the 1990s and enabled a dramatic increase in the channel density achievable with gaseous timing detectors. An MRPC consists of a stack of high-resistivity glass plates separated by sub-millimetre gas gaps. An applied high voltage (~ 15 kV) creates a uniform electric field across all gaps simultaneously; a traversing charged particle triggers an avalanche that propagates across several gaps, producing a

fast differential signal. The key readout electronics were the NINO ASIC [6], an ultra-fast differential amplifier-discriminator fabricated in $0.25\ \mu\text{m}$ CMOS, and the HPTDC (High-Performance Time-to-Digital Converter) [7], which achieved 25 ps binning over a large dynamic range (Fig. 4). Together they constituted the first fully ASIC-based timing readout in a major collider experiment.

The ALICE Time-of-Flight system at the LHC [8] deployed this technology at a scale previously impossible with PMT-based systems: $140\ \text{m}^2$ of active area, 157 888 readout channels, and a time resolution of ~ 80 ps at the system level (better than 60 ps for the MRPC strips alone). The stringent requirements – large area, high segmentation, low material budget, and a cost ceiling – could not have been met by scintillator-PMT technology, making the ALICE TOF a decisive proof-of-concept for large-scale ASIC-driven timing.

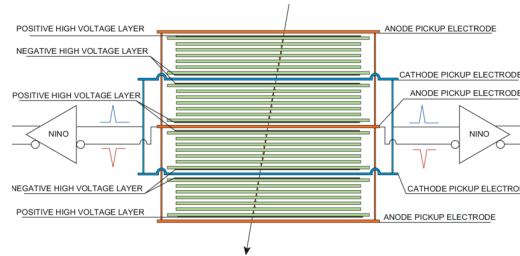


Figure 4: Schematic cross-section of a Multigap Resistive Plate Chamber (MRPC). Multiple high-resistivity glass plates (green) are interleaved with sub-millimetre gas gaps. The uniform electric field across all gaps simultaneously amplifies the avalanche initiated by a traversing particle. Differential signals from the anode and cathode pickup electrodes are fed directly into the NINO ASIC discriminators (shown at left and right), followed by an HPTDC for time digitisation. This readout chain enabled the ALICE TOF to achieve ~ 80 ps resolution across $140\ \text{m}^2$ of active area [8].

2.5. The Cherenkov family: DIRC and TOP

The BaBar [9] and Belle II [10] experiments at the B -factory colliders required compact, low-mass PID systems capable of π/K separation in an environment where a conventional TOF approach would have been physically impossible. Both solutions exploit the propagation of Cherenkov photons inside a quartz radiator.

The Detection of Internally Reflected Cherenkov light (DIRC) detector of BaBar used 144 fused-silica bars of length 4.9 m; photons were transported by total internal reflection to a water-filled standoff box instrumented with conventional PMTs, achieving ~ 2 mrad angular resolution per photon.

The Time-of-Propagation (TOP) counter of Belle II measures both the arrival time and the lateral position of Cherenkov photons at the end of a 2.5 m quartz plate read out by micro-channel plate PMTs with ~ 100 ps single-photon resolution. Since the path length inside the quartz depends on the Cherenkov angle and hence on the particle velocity, a single time measurement encodes the Cherenkov angle. Pions and kaons of the same momentum travel at slightly different velocities, producing photons at slightly different angles and therefore arriving with different delays; with a per-track time resolution below 50 ps the TOP counter provides $> 3\sigma$ K/π separation up to $\sim 4\ \text{GeV}/c$.

Table 1 summarises the principal timing systems of this era. The common features are: $\mathcal{O}(100)$ ps resolution, $\mathcal{O}(100)$ – $\mathcal{O}(10^5)$ readout channels, and a reliance on PMTs as the photo-

| Experiment | Technology | Area / Channels | Resolution | Primary use |
|------------------|------------------------|------------------------------|--------------|-------------------------|
| CDF-II TOF | Scint. + fine-mesh PMT | 216 bars | ~100 ps | PID (K/π) |
| NA48 hodoscope | Scint. + PMT | ~150 channels | ~150 ps | Pile-up rejection |
| AMS-02 TOF | Scint. + PMT | 34 paddles | ~160 ps | Trigger, directionality |
| ALICE TOF | MRPC (gaseous) | 140 m ² , 157 888 | ~80 ps | Hadron PID |
| Belle II TOP | Quartz + MCP-PMT | 16 modules | <50 ps/track | PID (K/π) |
| Super-K PMT wall | Water Cherenkov + PMT | 11 146 PMTs | ~2 ns/PMT | Vertex, direction |

Table 1: Representative timing systems of the 1990s and 2000s. The MRPC-based ALICE TOF was the first large-scale ASIC-driven timing system and bridged the gap to the silicon era.

sensor. The MRPC/NINO/HPTDC line pioneered ASIC-based readout and large-scale gaseous timing, presaging the silicon era.

3. The Silicon Revolution

The limitations of PMT-based systems – bulk, fragility, high-voltage requirements, sensitivity to magnetic fields, and limited granularity – became incompatible with the requirements of the next generation of experiments. Three inventions, developed in the 2000s and 2010s, removed these constraints: the SiPM for photon detection, the LGAD for direct charged-particle detection, and the deep-submicron timing ASIC.

3.1. Silicon Photomultiplier (SiPM)

A Silicon Photomultiplier is an array of tens to hundreds of thousands of Single-Photon Avalanche Diode (SPAD) microcells, each operating in Geiger mode, connected in parallel on a common substrate [11] (Fig. 5). When a photon liberates an electron-hole pair in a SPAD biased a few volts above breakdown, the resulting Geiger discharge produces a stereotyped charge pulse of $\sim 10^6$ electrons in ~ 1 ns. The sum of all firing cells constitutes an analog output proportional to the number of incident photons, provided the number of photons is much less than the number of cells.

SiPMs match or exceed the photon-detection efficiency of alkali PMTs (>40% peak), while operating at only 30–60 V bias compared to the 1–2 kV required by PMTs. Their millimetre-scale footprint allows tight coupling to crystal scintillators, they are immune to magnetic fields, and their unit cost at volume has fallen dramatically with CMOS foundry production. These properties make them the photosensor of choice for scintillator-based timing systems at the HL-LHC and beyond.

Scintillation and Cherenkov light with SiPMs. When a charged particle traverses a dense medium it can produce two distinct types of light, each with different temporal characteristics and timing implications. *Scintillation light* is emitted isotropically with a characteristic fluorescence lifetime of the crystal (a few nanoseconds for LYSO, ~ 40 ns for BGO), and is therefore delayed and spread in time. *Cherenkov light* is emitted promptly (< 1 ps) in a forward cone at angle $\cos \theta_C = 1/n\beta$, and represents a nearly instantaneous signal that can, in principle, reach sub-100 ps timing even from a single detected photon.

Three readout geometries exploit these two components differently, as illustrated in Fig. 6:

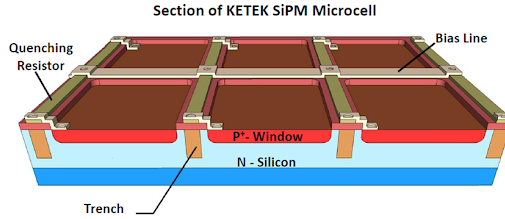


Figure 5: Three-dimensional cross-section of a KETEK SiPM microcell, showing the individual SPAD structure: the P⁺ window (active region) on N-silicon bulk, the trench isolation between cells, and the bias/quenching resistor network on the surface. Each microcell fires independently in Geiger mode; the parallel sum of all cells gives an analog output proportional to the number of incident photons. Modern SiPMs integrate 10^3 – 10^4 such cells per mm².

1. Scintillation only. SiPMs are mounted on the lateral faces of a crystal bar. Scintillation light bounces along the bar and reaches the SiPMs after multiple reflections, producing a large but temporally broadened signal. The Cherenkov cone is directed along the particle trajectory toward the bar ends and is not collected; the timing is dominated by the crystal decay time.
2. Scintillation and Cherenkov. The SiPM is placed at the end of the crystal, aligned with the particle direction. Cherenkov photons emitted in the forward cone arrive at the SiPM promptly and directly; scintillation photons arrive later after diffuse propagation. The Cherenkov component provides a fast leading edge, while the slower scintillation component yields the energy measurement. This dual-component signal is the basis of precision timing in PbWO₄ and PbF₂ crystals.
3. Cherenkov only in the SiPM. At sufficiently high particle velocity, Cherenkov light is generated directly inside the SiPM silicon substrate or its protective window, without any external crystal. Only a handful of photons are produced, but they arrive with sub-picosecond jitter. This effect, while difficult to exploit at low energies, sets an intrinsic physical lower bound on the timing resolution achievable with SiPM-based detectors.

The principal limitations of SiPMs for timing are correlated noise (after-pulsing, optical cross-talk) and the capacitance of large-area devices, which degrades the signal-to-noise ratio when the cell count is large. The latest SiPM productions have a reduced dark-count rates, ~ 100 kcps/mm² at 20°C, an important figure for the low-photon-count regime of Cherenkov readout.

3.2. Low-Gain Avalanche Diode (LGAD / UFSD)

While SiPMs detect photons via Geiger-mode operation, a different silicon structure is required to detect the direct ionisation signal from a charged particle. The Low-Gain Avalanche Diode (LGAD) design [12] (Fig. 7) is the key technological step that allows the design of silicon sensors with high temporal resolution, also known as Ultra-Fast Silicon Detector (UFSD) [13]. This technology uses a thin implanted p⁺ gain layer to provide an internal multiplication factor of 10–30.

A MIP traversing a 50–300 μm thick LGAD deposits ~ 70 –2000 electron-hole pairs. Internal multiplication raises this to a collected charge of 5–20 fC, producing a fast current pulse with a rise time below 1 ns. The combination of high signal amplitude and fast rise time yields an excellent signal-to-noise ratio and, critically, allowed to reduce the electronic jitter below 30 ps [14].

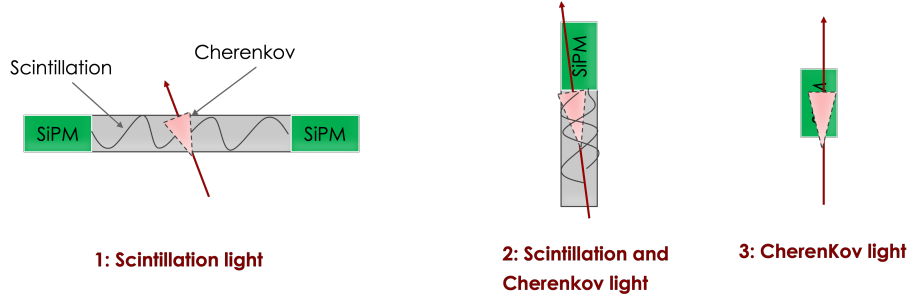


Figure 6: Three configurations for SiPM-based optical timing. (1) *Scintillation only*: SiPMs on the lateral sides of a crystal bar collect isotropic scintillation light after multiple reflections; the Cherenkov cone directed along the bar axis is not collected. This geometry maximises the number of detected photons but the timing is limited by the crystal fluorescence lifetime. (2) *Scintillation and Cherenkov*: the SiPM is placed at the end of the crystal, along the particle direction; forward Cherenkov photons arrive promptly and directly, providing a fast timing signal, while scintillation photons arrive later and give the energy measurement. (3) *Cherenkov only*: Cherenkov light produced directly in the SiPM package or a thin radiator provides a purely prompt signal with very few photons, representing the ultimate timing limit of the technology.

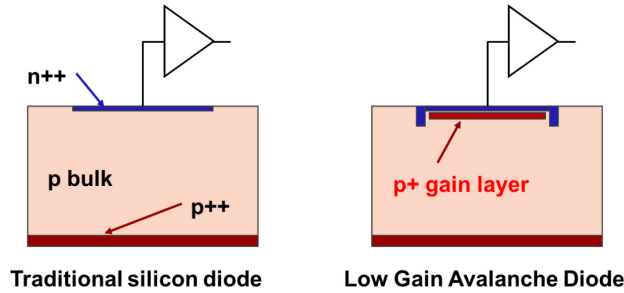


Figure 7: Schematic cross-sections comparing a traditional silicon diode (left) and a Low-Gain Avalanche Diode (right). In the LGAD, a thin p^+ gain layer implanted just below the n^{++} electrode creates a localised high-field region that provides internal multiplication of factor 10–30. This moderate gain is sufficient to produce fast current pulses with excellent signal-to-noise ratio, enabling time resolutions of 25–40 ps per layer [12].

The temporal resolution σ_t of an UFSD is decomposed into two independent contributions [14]:

$$\sigma_t^2 = \sigma_{\text{jitter}}^2 + \sigma_{\text{Landau Noise}}^2 \quad (1)$$

- Jitter arises from electronic noise σ_N and the signal slew rate dV/dt at threshold crossing, $\sigma_{\text{jitter}} = \frac{\sigma_N}{dV/dt}$. It dominates at low gain, where the signal amplitude is small relative to the noise.
- Landau noise, also called the non-uniform ionization term, arises from the event-to-event variability of the charge deposition. Each MIP deposits charge in a different spatial pattern along the track, producing a different signal shape and hence a different trigger time. This term dominates at high gain, where jitter is negligible. The Landau noise grows with the square root of the thickness d and decreases with drift velocity v , $\sigma_{\text{Landau Noise}} \propto \sqrt{d}/v$. Operating at fields sufficient to saturate the drift velocity v , and reducing sensor thickness,

are the most effective ways to reduce this term. Sensors with a thickness is in the range 35–55 μm have an intrinsic resolutions of 15–25 ps.

Radiation hardness is a critical parameter for collider applications. The gain layer is composed of boron acceptors that are progressively deactivated by proton and neutron irradiation through the acceptor removal mechanism [15]. UFSDs retain useful gain up to fluences of $\sim 2 \times 10^{15} \text{ n}_{\text{eq}}/\text{cm}^2$, sufficient for the HL-LHC applications; higher fluence applications require alternative geometries described below.

3.3. Resistive Silicon Detector (RSD / AC-LGAD)

The Resistive Silicon Detectors (RSDs) are an UFSD variant in which the n^+ electrode is replaced by a continuous resistive layer, and the readout pads are connected in AC or DC mode to the surface [16]. When a MIP hits the sensor, the signal spreads laterally under the resistive layer before being read by the nearest electrodes. By measuring the charge fraction on each electrode, the hit position can be reconstructed with a precision below 5% of the pixel size, far better than the electrode pitch. The position reconstruction relies on the fact that the resistive layer acts as a two-dimensional impedance network. When a MIP hits the sensor at a point surrounded by n readout electrodes, each at impedance distance Z_i from the hit, the signal fraction collected by electrode i is

$$S_i \propto \frac{1/Z_i}{\sum_{k=1}^n 1/Z_k}, \quad (2)$$

as illustrated in Fig. 8.

RSD thus decouples the spatial resolution from the electrode granularity, using a fraction of the power and readout complexity of an equivalent array of small standard LGADs. This property makes RSD attractive for applications where the power budget or the number of readout channels must be minimised.

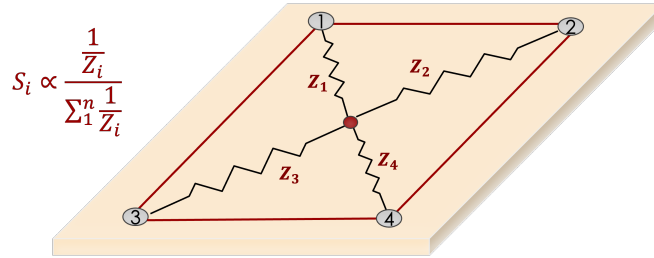


Figure 8: Operating principle of the Resistive Silicon Detector (RSD). A MIP hits the continuous resistive surface at the red dot, and the induced signal spreads to the four corner electrodes (1–4) through the resistive network with impedances Z_1 – Z_4 . The fraction of the total charge collected by each electrode is $S_i \propto (1/Z_i) / \sum_k (1/Z_k)$, where Z_i is proportional to the distance from the hit to electrode i .

Table 2 present a summary of the silicon sensors used for timing.

| Technology | Detection | Gain | Timing resolution |
|-------------------|-------------------|--------------------------|-------------------|
| SiPM | Photon (indirect) | 10^5 – 10^6 (Geiger) | <100 ps / photon |
| LGAD / UFSD | MIP (direct) | 10–30 (linear) | 25–40 ps / layer |
| RSD / AC-LGAD | MIP (direct) | 10–30 (linear) | 25–40 ps / layer |
| Standard silicon | MIP (direct) | 1 (no gain) | >200 ps |
| 3D trench silicon | MIP (direct) | 1–low | ~10 ps (lab) |

Table 2: Silicon sensors presently used for timing.

4. From 3+1 to 4D Tracking

4.1. The conceptual shift

In all the experiments discussed so far, timing was a *dedicated* measurement confined to a specific detector subsystem: a timing layer, a TOF wall, a hodoscope. The tracking detector itself provided only position information, and timing was added as a separate coordinate, useful but not integrated into the event reconstruction.

The availability of SiPMs, LGADs, and timing ASICs makes a qualitatively different use of timing possible. The concept of 4D tracking adds time as a fourth coordinate measured at *every point* along the track, alongside the three spatial coordinates. This is to be distinguished from the simpler 3+1 tracking, in which a timing layer provides a single time measurement per track, assigned during final reconstruction.

4.2. The 4D tracking challenge

The optimisation of a 4D system is not a single-variable problem. Five parameters must be balanced simultaneously: temporal resolution, spatial resolution and pixel size, material budget, occupancy, and radiation level. These parameters are deeply intertwined, and improving one invariably degrades at least one other. As a consequence, no single sensor technology is optimal for all applications, and the landscape of 4D detectors is necessarily diverse. Figure 9 illustrates the four dominant trade-offs.

Power and timing resolution. The ASIC power budget is the central bottleneck. Achieving good timing requires a fast, low-noise amplifier (large bias current) and a high-frequency TDC (large dynamic power). In 28 nm CMOS, a per-pixel TDC operating at the ~10 ps level consumes ~1.5–2 W/cm². The maximum power that can be removed by an evaporative CO₂ cooling circuit with acceptable material budget is ~0.3–0.5 W/cm², a shortfall of a factor four to six that is the dominant engineering challenge for next-generation trackers. Relaxing the timing requirement to ~25–30 ps (HL-LHC level) reduces the power to a manageable ~0.2–0.4 W/cm², which is why HL-LHC timing layers are feasible today whereas a full 4D inner tracker is not yet.

Power and material budget. Every watt of heat dissipated in the detector volume requires a cooling circuit. A standard evaporative CO₂ system contributes ~0.5–1% X_0 per cooling loop, which is comparable to or larger than the sensor itself. For inner tracker layers, where the total material budget target is often $O(1\%) X_0$ per layer, the cooling infrastructure can dominate the material budget and undo the gains from using thin sensors. This coupling between power and material is one of the strongest arguments for the monolithic CMOS-LGAD approach (Section 6.4), where the lower power density makes air cooling viable and eliminates the CO₂ circuit entirely.

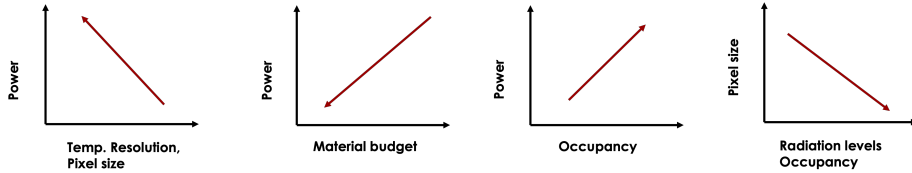


Figure 9: The four fundamental trade-offs in the optimisation of a 4D silicon tracking sensor. *First*: power consumption increases as timing resolution improves and pixel size decreases – faster front-end amplifiers and higher-frequency TDC oscillators consume more current, and finer granularity means more channels per unit area. *Second*: higher power requires more cooling infrastructure (CO₂ circuits, support structures), directly increasing the material budget and therefore the multiple-scattering contribution to spatial resolution. *Third*: higher occupancy environments demand more power, because front-end circuits must process hits at higher rates without dead time. *Fourth*: harsher radiation environments and higher occupancy force the use of smaller pixels to limit per-pixel hit rates and to maintain spatial resolution after radiation damage, but smaller pixels amplify the power and material problems. Each experiment sits at a different point in this multi-dimensional space, making a universal 4D solution impossible.

Occupancy and power. High-occupancy environments – the inner layers of high-luminosity collider detectors – require front-end electronics that can sustain high hit rates without saturation or dead time. Sustaining low dead time at high hit rates requires larger buffers, faster serialisers, and higher-bandwidth data links, all of which increase power. The LHCb VELO Upgrade II inner region, with ~ 800 tracks per crossing at 5 mm from the beam, represents the current extreme of this trade-off.

Radiation, occupancy, and pixel size. Radiation damage degrades the charge collection efficiency and increases the leakage current of silicon sensors; both effects worsen as the fluence increases. Reducing the pixel area limits the leakage current per channel (improving the signal-to-noise ratio) and reduces the per-pixel occupancy, preserving spatial resolution. However, smaller pixels mean more channels per unit area, more ASICs, more power, and more material. The minimum viable pixel size is therefore set by a balance between the radiation hardness requirement and the power/material budget, a balance that shifts with every new ASIC process node. At present, $55 \times 55 \mu\text{m}^2$ at 28 nm represents the practical frontier for inner vertex detectors at the LHC (LHCb VELO Upgrade II); future colliders will likely require $20 \times 20 \mu\text{m}^2$ or below, motivating the move to 14 nm or 7 nm CMOS processes.

5. Timing Systems Under Construction

5.1. CMS MIP Timing Detector (MTD)

The CMS experiment at the HL-LHC will install the MIP Timing Detector (MTD) in Phase-2 [19]. The MTD provides one time measurement per track (3+1 mode) for pile-up rejection at $\langle \mu \rangle = 200$. The detector occupies 4.5 cm of radial space in the barrel (Barrel Timing Layer, BTL) and 9.9 cm of longitudinal space in the endcap (Endcap Timing Layer, ETL).

| System | Technology | Area | Channels | σ_t goal |
|-------------|--------------------------|--------------------|----------|------------------|
| CMS MTD BTL | LYSO + SiPM + TOFHIR2 | 38 m ² | 350 k | 30–60 ps |
| CMS MTD ETL | LGAD + ETROC (65 nm) | 14 m ² | 8.5 M | 30–40 ps |
| ATLAS HGTD | LGAD + ALTIROC (130 nm) | 6.4 m ² | 3.5 M | 25–35 ps |
| CMS HGCAL | Si + SiPM tiles + HGCROC | endcap | ~6 M | ~30 ps (cluster) |

Table 3: Timing systems under construction for the HL-LHC (installation ~2028–2030).

Barrel Timing Layer (BTL). The BTL uses LYSO:Ce crystal scintillator bars ($3.75 \times 3.75 \times 57$ mm³) read out by SiPMs on both ends. The total active area is ~ 38 m² with ~ 350 000 channels. The TOFHIR2 ASIC [20] (130 nm CMOS) provides ToA and charge measurements and targets a time resolution of 30 ps (beginning of life) to 60 ps (end of life, after irradiation degrades the crystal light yield).

Endcap Timing Layer (ETL). The ETL uses LGAD sensors of 1.3×1.3 mm² pixel size in a double-disk geometry, covering ~ 14 m² with ~ 8.5 million channels. The ETROC ASIC [21] (65 nm CMOS) provides ToA with ToT-based time-walk correction and targets ~ 25 ps electronics jitter, contributing to a system-level goal of ~ 30 – 40 ps per track. Evaporated CO₂ cooling manages the ASIC power density within the tight material budget allowed in the tracker volume.

5.2. ATLAS High-Granularity Timing Detector (HGTD)

The ATLAS Phase-2 upgrade includes the High-Granularity Timing Detector (HGTD) [22], positioned in front of the endcap calorimeter at $|z| = 3.5$ m. It covers $2.4 < |\eta| < 4.0$ with LGAD pixels of 1.3×1.3 mm², for a total active area of ~ 6.4 m² and ~ 3.5 million channels. The ALTIROC ASIC [24] (130 nm CMOS) provides a target time resolution of ~ 35 ps per layer, read out with two sensor layers per disk for a total per-track resolution of ~ 25 ps after combination. Like the CMS ETL, the HGTD uses evaporated CO₂ cooling integrated within the detector structure.

5.3. CMS High-Granularity Calorimeter (HGCAL)

The CMS HGCAL [25] replaces the existing endcap calorimeter with a sampling imaging calorimeter consisting of 47 layers alternating silicon sensors and scintillator tiles read out by SiPMs. In the electromagnetic section, the active elements are hexagonal silicon sensors of 0.5–1.1 cm² cell size; in the hadronic section, SiPM-on-scintillator tiles provide timing alongside energy measurement. The timing performance goal is ~ 30 ps for electromagnetic clusters with energy above 5 GeV, sufficient to reject out-of-time pile-up and to associate electromagnetic showers with the correct primary vertex. The primary function is rejecting “halo” hits – energy deposits from out-of-time pile-up particles that arrive at the calorimeter with a time offset of ± 3 ns. A 30 ps timing cut retains $>99\%$ of genuine in-time showers while suppressing the pile-up contribution, improving jet energy resolution in the 200-pile-up environment by $\sim 20\%$, as shown in Fig. 10.

The key parameters of all HL-LHC timing systems are collected in Table 3.

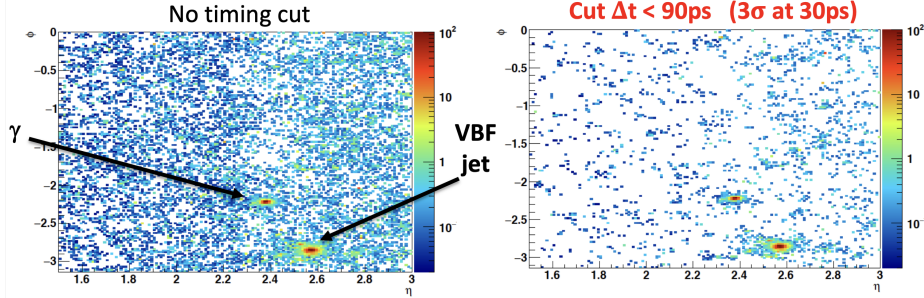


Figure 10: Effect of a 90 ps timing cut (3σ at 30 ps resolution) on HGCAL occupancy. Left: the (η, ϕ) map of energy deposits without any timing selection, showing a dense background of out-of-time pile-up hits throughout the endcap. Right: after applying $|\Delta t| < 90$ ps, the pile-up halo is almost entirely removed while the in-time VBF jet and photon candidates are preserved [25].

6. Timing in New and Near-Future Experiments

6.1. PIONEER at PSI

PIONEER [26] is a proposed rare pion decay experiment at the Paul Scherrer Institute, aiming to measure $\mathcal{B}(\pi^+ \rightarrow e^+ \nu) / \mathcal{B}(\pi^+ \rightarrow \mu^+ \nu)$ at 0.01% precision, a factor of fifteen improvement on the current world average. The central challenge is suppressing the $\pi \rightarrow \mu \rightarrow e$ decay chain background, in which the pion stops and decays to a muon, which in turn decays to a positron, all within a few hundred picoseconds and within the same spatial volume of the active target.

The Active TARget (ATAR) of PIONEER uses an AC-LGAD (RSD) stack to perform decay-chain topology reconstruction in four dimensions. With a per-layer time resolution of < 100 ps, the system distinguishes the stopping π^+ signal from the subsequent μ^+ signal and the final e^+ signal as separate hits displaced in time even when they are spatially coincident. The readout ASIC is FAST3 [42], a front-end with ~ 30 ps resolution designed to read out thin LGADs, providing ToA and charge measurements.

6.2. Electron-Ion Collider (EIC / ePIC)

The Electron-Ion Collider at Brookhaven National Laboratory [27] will begin operation in the early 2030s, using the ePIC detector for its first physics programme. Timing is essential for particle identification across a wide momentum range in the hadronic final state.

The ePIC Time-of-Flight system uses AC-LGAD (RSD) sensors for the barrel and forward regions. The barrel TOF consists of RSD strips targeting a time resolution of 25–35 ps, read out by the EICROC ASIC (130 nm CMOS) [28]. The forward TOF uses 0.5×0.5 mm² RSD pixels for high-rate 4D tracking. Together these provide 3σ $\pi/K/p$ separation over the relevant momentum range, with a flight path of ~ 1 m. EICROC measures both Time-of-Arrival (ToA) and pulse amplitude (charge), the latter being essential for the position reconstruction algorithm of AC-LGAD sensors.

6.3. LHCb VELO Upgrade II: the first 4D vertex detector

The LHCb upgrade for Long Shutdown 4 (~ 2034) will replace the current Vertex Locator with a full 4D tracker – the first application of per-hit timing in a collider vertex detector [29]. The operating environment is extreme: radiation fluence up to 6×10^{16} n_{eq}/cm² at 5 mm from

| Experiment | Technology | Mode | σ_t goal | Key challenge |
|----------------------|----------------------|------------------|-----------------|------------------------|
| PIONEER (PSI) | AC-LGAD (RSD) | 4D active target | <100 ps | Decay chain separation |
| ePIC (EIC) | AC-LGAD (RSD) | TOF + 4D | 25–35 ps | PID, momentum range |
| LHCb VELO Upgrade II | 3D Trench + LGAD | 4D vertex | ~20 ps/hit | Radiation, power |
| ALICE 3 | Monolithic CMOS-LGAD | 4D tracking | ~20 ps | Material, area, power |

Table 4: Silicon timing detectors for new and near-future experiments.

the beam, very high track occupancy (~ 800 tracks per crossing in the inner region), and a strict power budget. The total active area is $\sim 0.15 \text{ m}^2$.

The sensor technology uses 3D Trench Silicon sensors for the innermost region, where LGAD gain would be entirely lost by radiation damage, and LGAD or planar sensors for the outer region. Pixel size is $55 \times 55 \mu\text{m}^2$. The PICOPIX ASIC (28 nm CMOS) [30] implements the *Analogous Island* concept, in which analogue shaping and TDC resources are shared among clusters of pixels, reducing the per-pixel power below the threshold sustainable by the CO_2 evaporative cooling, while maintaining a time resolution of ~ 20 ps. With 7–10 timing layers per track, the VELO Upgrade II will perform full 4D vertexing with a vertex time resolution of ~ 7 –10 ps.

6.4. ALICE 3

ALICE 3 [31] represents the opposite extreme from LHCb: a nearly massless 4D tracker for a low-radiation, large-area environment. The physics programme requires pion-kaon separation at momenta below 1 GeV/c, demanding TOF measurements with a system resolution approaching 20 ps over a flight path of a few centimetres. The total active area is $\sim 45 \text{ m}^2$.

The sensor concept is a Monolithic CMOS-LGAD (for example, the ARCADIA or MADPix projects), in which the gain layer and readout electronics are integrated on the same silicon die using a commercial CMOS process. The monolithic approach avoids the bump-bonding step needed for hybrid assemblies, reducing the material budget to $\mathcal{O}(0.1\%) X_0$ per layer. Power consumption is targeted below 40 mW/cm^2 , feasible with air cooling, enabling the cylindrical bent geometry required by the ALICE 3 design. Table 4 summarises the key parameters of these detectors.

7. Timing in Far-Future Experiments

The far-future experiments at proposed facilities push timing requirements to their physical limits, demanding a further factor of three to five improvement in per-hit resolution compared to current HL-LHC systems.

7.1. FCC-ee

The Future Circular Collider in the electron-positron mode (FCC-ee) [32] is a precision electroweak, flavour, and Higgs factory. The TOF system targets ~ 10 ps per track for $3\sigma K/\pi$ separation up to $\sim 5 \text{ GeV}/c$. Without this capability, the flavour physics programme would be limited by kaon-pion misidentification in multi-body B decays. Candidate technologies include LGAD-based TOF layers or TORCH-like detectors. The calorimetry, discussed in Section 8, also uses timing in the dual-readout mode for longitudinal shower profiling.

| Facility | Pile-up / BIB challenge | σ_t target | Primary motivation |
|------------|-------------------------|-------------------|------------------------------------|
| FCC-ee | Low (clean e^+e^-) | ~ 10 ps | PID (K/π), dual-readout cal. |
| Muon Coll. | BIB (>99% rejection) | 20–30 ps | Tracker: BIB gating |
| Muon Coll. | BIB | ~ 80 ps | Calorimeter: BIB gating |
| FCC-hh | $\mu \approx 1000$ | < 10 ps | Vertex reconstruction |

Table 5: Timing requirements for far-future facilities.

7.2. Muon Collider

A Muon Collider at centre-of-mass energies of several TeV [34] faces a unique background environment: muons decay continuously along the accelerating and storage ring, producing a flux of electrons, photons, and neutrons (Beam-Induced Background, BIB) that arrives at the detector *asynchronously* with the colliding bunch. The BIB rate is several orders of magnitude higher than the physics rate, and its particles have a broad time distribution spanning ± 10 ns around the collision.

Timing is the primary tool for BIB suppression. A gate of ± 150 ps around the collision time, feasible with 20–30 ps per-hit resolution, removes >99% of BIB hits from the tracker. Without this, the detector occupancy would be nearly 100% and event reconstruction would be impossible. The vertex detector targets 20–30 ps, while the calorimeter aims for 80 ps per cell (Section 8).

7.3. FCC-hh

The hadron mode of the FCC (FCC-hh) [33] targets a centre-of-mass energy of 100 TeV with a pile-up of ~ 1000 simultaneous proton-proton interactions per bunch crossing. At such pile-up densities, spatial tracking alone becomes increasingly challenged in resolving primary vertices along the beam axis. Design studies indicate that per-hit time resolutions approaching or below 10 ps would substantially improve vertex separation in a combined “Time-Z” reconstruction, where both spatial and temporal coordinates are used for track association. Reaching this level of performance motivates continued development of advanced CMOS nodes (28 nm and beyond) together with sensor concepts targeting single-hit resolutions well below 10 ps. Values in the few-picosecond regime are currently considered long-term R&D objectives rather than demonstrated detector-level performance under realistic radiation and power constraints.

The timing requirements of these facilities are compared in Table 5.

8. Timing in future Calorimeters

Calorimeters have traditionally sacrificed time resolution for energy resolution; modern systems are reversing this priority, treating timing as an essential tool for shower cleaning, pile-up rejection, and longitudinal profiling.

8.1. LHCb PicoCal

The LHCb calorimeter Upgrade II (PicoCal) is a multi-technology proposal targeting ~ 20 ps per cluster. It combines two readout geometries:

| System | Technology | σ_t goal | Primary timing role |
|-------------------|--|-----------------------------|------------------------|
| LHCb PicoCal | SpaCal / Shashlik + SiPM | ~ 20 ps per cluster | Shower separation |
| Crilin (Mu Coll.) | PbF ₂ /PbWO ₄ + SiPM | < 25 ps for $e^- > 3$ GeV | BIB gating |
| IDEA (FCC-ee) | Dual-readout fibres + SiPM | < 100 ps per fibre | Longitudinal profiling |
| Mu Coll. ECal | Fast crystals + SiPM | ~ 80 ps per cell | BIB gating |

Table 6: Calorimeter timing systems: present construction and future plans.

- *SpaCal* (Spaghetti Calorimeter): tungsten/lead absorber with scintillating fibres read out by SiPMs.
- *Shashlik*: scintillator/lead stacks with wavelength-shifting fibres, also SiPM-read.

The goal is to separate overlapping electromagnetic showers in the high-occupancy central region of LHCb at Upgrade II luminosities.

8.2. Crilin for the Muon Collider

The Crilin crystal calorimeter [37] has been developed specifically for the BIB environment of the Muon Collider. It uses PbF₂ (pure Cherenkov) or ultra-fast PbWO₄ crystals read out by SiPMs. Test beam measurements have demonstrated < 25 ps for electrons above 3 GeV. Since BIB particles arrive with a broad time distribution, while physics products arrive within ± 150 ps of the collision, a per-cell resolution of ~ 25 – 50 ps provides effective BIB gating in the calorimeter. This is the calorimetric analogue of the tracking BIB gate described in Section 7.2.

8.3. Dual-readout calorimetry: IDEA / FCC-ee

The dual-readout approach (IDEA detector at FCC-ee, HiDRa and ASPIDES projects [38]) reads out both Scintillation and Cherenkov light from the same fibre matrix simultaneously. The Scintillation signal integrates over the full hadronic shower; the Cherenkov signal responds only to the electromagnetic component. The ratio of the two signals, combined with a model of hadronic shower development, determines the electromagnetic fraction and hence corrects for the intrinsic non-compensation of the sampling calorimeter.

Timing adds a third dimension: the Cherenkov signal is prompt (< 1 ns), while scintillation is delayed by the fluorescence lifetime (~ 2 – 5 ns for fast crystals, longer for doped fibres). By measuring the arrival time of each fibre signal with < 100 ps resolution, the system reconstructs the longitudinal position of the shower centre without physical longitudinal segmentation. The readout electronics target < 100 ps per fibre using SiPMs coupled to ASICs such as Citiroc or dedicated TDC chips.

Table 6 summarises the calorimeter timing systems described in this section.

9. Timing in future Gaseous and Cherenkov detectors

Gaseous and Cherenkov timing technologies retain important roles in the future landscape, particularly where large areas must be covered at low cost, or where particle identification is required over macroscopic flight paths.

| System | Technology | σ_t | Application | Status |
|-------------------------|------------------------------|---------------------|---------------------|--------------------|
| ALICE TOF (Run 1–2) | MRPC + NINO + HPTDC | ~ 80 ps | Hadron PID | Operational |
| Belle II TOP | Quartz + MCP-PMT | < 50 ps/track | K/π PID | Operational |
| TORCH (LHCb Upgrade II) | Quartz + MCP-PMT | ~ 15 ps/track | $K/\pi, p/K$ | R&D / construction |
| PICOSEC Micromegas | MgF ₂ + CsI + gas | < 25 ps | Large-area TOF wall | R&D |
| 4D-RICH | MCP-PMT + Timepix4 | ~ 30 ps/photon | RICH enhancement | R&D |

Table 7: Gaseous and Cherenkov timing systems.

9.1. TORCH at LHCb Upgrade II

TORCH [39] will be installed in LHCb for Upgrade II. It uses 1 cm thick fused-silica quartz plates as Cherenkov radiators and Micro-Channel Plate PMTs (MCP-PMT) for photon detection. The system reconstructs the time-of-flight of a charged particle over a flight path of 9.5 m downstream of the interaction point. A per-photon resolution of ~ 70 ps from the MCP-PMTs combines over ~ 30 detected photons per track to yield a per-track resolution of ~ 15 ps. This provides 3σ K/π separation up to 10 GeV/ c and p/K separation up to 15 GeV/ c , complementing the silicon TOF layers for high-momentum PID. Readout is provided by waveform-digitizer ASICs of the ASOC/SAMPIC family.

9.2. PICOSEC Micromegas

The PICOSEC Micromegas [40] is a hybrid gaseous detector combining a Cherenkov radiator (MgF₂) and a photocathode (CsI) with a two-stage Micromegas amplification gap. A charged particle generates Cherenkov photons in the MgF₂ window; these liberate photoelectrons from the CsI photocathode, which are pre-amplified in the first (“drift”) gap and further amplified in the Micromegas gap. The resulting signal has a rise time of ~ 1 ns, yielding a consistently measured resolution of < 25 ps for MIPs.

PICOSEC is proposed for large-area forward timing walls where the cost of silicon would be prohibitive. Its radiation hardness exceeds that of conventional MRPCs, and the gas amplification gain can be tuned to compensate for photocathode ageing.

9.3. 4D-RICH

Several projects are exploring the addition of timing to Ring-Imaging Cherenkov (RICH) detectors. By coupling an MCP-PMT to a Timepix4 pixelated anode [41], single-photon timing of ~ 30 ps becomes achievable, enabling the per-photon timestamps to be used as an additional filter against background photons. In environments such as ALICE 3 or LHCb Upgrade II, where the occupancy per ring is high, rejecting photons whose arrival time is inconsistent with the track time reduces the combinatorial background in ring finding significantly. The concept is being developed under the name “4D-RICH” project.

Table 7 summarises gaseous and Cherenkov timing systems past and future.

10. Timing in future Satellite Experiments

Space-borne cosmic-ray detectors impose constraints qualitatively different from those of ground-based particle physics experiments, and timing in space has its own unique requirements. The primary drivers are: particle identification and isotope separation via TOF, charge

measurement via dE/dx , directionality determination, and a strict power budget typically below 20 mW/cm^2 .

Experiments such as AMS-02 (Section 2.1), DAMPE, and future planned missions use TOF measurements for:

- PID and isotope separation: distinguishing, for example, ^3He from ^4He on the basis of their velocity at the same rigidity. The mass-squared difference scales as $(M_A^2 - M_B^2)/p^2$; for helium isotopes at a few GV of rigidity, this requires a TOF resolution of $O(100)$ ps over a flight path of ~ 1 m.
- Directionality and self-veto: as in AMS-02, the top-to-bottom time difference between two silicon tracker layers determines whether a particle is entering from above (cosmic ray) or below (secondary), allowing a single silicon layer to function as a directional detector without a dedicated TOF scintillator. This is a direct application of 4D silicon sensing to the space environment.

Future satellite missions are evaluating thin LGAD layers as a replacement for scintillator/PMT TOF paddles, offering lower mass, lower voltage operation, and the possibility of fine-grained spatial information at the same time. The power constraint of $<20 \text{ mW/cm}^2$ is compatible with the low-power designs being developed for ALICE 3, making these two communities natural collaborators.

11. Timing ASICs

The development of the timing ASIC is arguably the most technically challenging aspect of the transition to silicon timing. While some design blocks are common for SiPMs and LGADs, ASICs for SiPM and LGAD readout differ substantially in several aspects such as the analogue front-end design (SiPM signals, $\sim 1\text{--}10$ pF capacitance, $\sim 1\text{--}4$ mA peak current, are qualitatively different from LGAD signals, $\sim 0.1\text{--}1$ pF, $\sim 10\text{--}100$ μA peak current) and specialized circuits such as the SiPM dark count suppression.

Table 8 summarises the principal chips discussed below.

11.1. The NA62 GigaTracker

The TDCPix ASIC developed for the NA62 GigaTracker [18] (Fig. 11) is widely regarded as the first of modern silicon timing ASICs. Fabricated in 130 nm CMOS, it provides Time-of-Arrival (ToA) measurements with ~ 100 ps time resolution across a $60 \times 27 \text{ mm}^2$ die containing 18 000 pixels of $300 \times 300 \mu\text{m}^2$. The GigaTracker operated at a beam rate of $\sim 1 \text{ MHz/mm}^2$ in the NA62 kaon beam, demonstrating for the first time that sub-100 ps timing [17] could be integrated directly into a high-rate pixel detector at moderate power consumption.

11.2. ASICs for the ATLAS and CMS timing layers at the HL-LHC

ETROC (CMS ETL). ETROC [21] is fabricated in 65 nm CMOS and provides Time-of-Arrival (ToA) and Time-over-Threshold (ToT) measurements for the CMS LGAD timing layer. The ToT information enables time-walk correction on-chip. Electronics jitter is targeted at ~ 25 ps. The ETROC2 prototype has demonstrated full functionality with LGAD sensors in test beams.



Figure 11: Photographs of a NA62 GigaTracker station, showing the sensor side (left) and the cooling plate side (right). The station houses a $60.8 \times 27 \text{ mm}^2$ hybrid pixel detector with $300 \times 300 \mu\text{m}^2$ pixels, read out by the TDCPix ASIC fabricated in 130 nm CMOS. Operating in the full NA62 kaon beam at $\sim 1 \text{ MHz/mm}^2$, the GigaTracker was the first demonstration that sub-100 ps timing could be integrated directly into a high-rate pixel detector, establishing the blueprint for all subsequent timing ASICs [18].

ALTIROC (ATLAS HGTD). ALTIROC [24] is fabricated in 130 nm CMOS and reads out the ATLAS LGAD disks. It uses a similar ToA + ToT architecture and targets a comparable electronics contribution to the overall 25–35 ps system resolution.

TOFHIR2 (CMS BTL). The TOFHIR2 ASIC [20] is designed for the CMS LYSO+SiPM barrel layer. It operates in 130 nm CMOS and reads out both timing and charge. A dedicated dark-count cancellation scheme suppresses SiPM thermal noise hits. The electronics contribution targets 30 ps at beginning of life, rising to ~ 60 ps as radiation damage increases SiPM dark count rates at end of life.

11.3. ASICs for EIC

AC-LGAD (RSD) sensors require ASICs that measure both ToA and pulse amplitude at each electrode, because the hit position is reconstructed from the charge ratio between neighbouring electrodes. This imposes a different analogue architecture from the standard LGAD readout.

EICROC. The EICROC [28] is a 130 nm ASIC developed by a consortium including BNL and Fermilab for the EIC forward TOF. It measures ToA and charge simultaneously and is designed for $0.5 \times 0.5 \text{ mm}^2$ pixels at the high hit-rate of the EIC forward region.

FCFD. The FCFD [23] (Fermilab, 65 nm CMOS) uses a constant-fraction discriminator to measure signal arrival time, avoiding the need for time-walk correction by design. It achieves ~ 10 ps electronics contribution for LGAD signals above 20 fC, aimed at barrel TOF applications.

11.4. Next-generation frontier: 28 nm ASICs

TIMESPOT1. TIMESPOT1 [35], developed by INFN, was the first 28 nm demonstrator ASIC for in-pixel TDC integration. It achieves a time resolution of ~ 7 ps per pixel for $55 \times 55 \mu\text{m}^2$ pixels – demonstrating that the intrinsic limit of a thin 3D silicon sensor can be reached at the ASIC level. The primary limitation is power density of $\sim 1.5\text{--}2 \text{ W/cm}^2$, which exceeds the sustainable limit for large-area detectors and motivates the resource-sharing strategies of successor chips.

| ASIC | Process | Electronics jitter | Sensor type | Application |
|-------------|-----------|--------------------|------------------|----------------------|
| ETROC | 65 nm | ~25 ps | LGAD | CMS MTD ETL |
| ALTIROC | 130 nm | ~30 ps | LGAD | ATLAS HGTD |
| TOFHIR2 | 130 nm | 30–60 ps | SiPM + Crystal | CMS MTD BTL |
| EICROC | 130 nm | ~30 ps | AC-LGAD | EIC ePIC TOF |
| FCFD | 65 nm | ~10 ps | LGAD / AC-LGAD | EIC ePIC TOF |
| TIMESPOT1 | 28 nm | ~7 ps | 3D Trench / LGAD | Demonstrator |
| PICOPIX | 28 nm | ~20 ps | 3D Trench / LGAD | LHCb VELO II |
| SAMPIC/ASOC | 130–65 nm | <10 ps | MCP-PMT / SiPM | TORCH, small systems |

Table 8: Summary of principal timing ASICs.

PICOPIX. PICOPIX [30] is developed within the Timepix family at CERN. It implements the *Analogue Island* concept, sharing TDC resources among groups of pixels and using power-gating techniques to reduce the average power to a sustainable level while maintaining ~20 ps timing. PICOPIX is the baseline readout ASIC for the LHCb VELO Upgrade II.

11.5. Alternative paths: waveform digitizers

For detectors with fewer channels (MCP-PMT arrays, small SiPM matrices), where the data volume is manageable, waveform digitizers offer the best possible timing. The ASOC and SAMPIC [36] chips sample the full pulse shape at ~1–8 GS/s (equivalent to a GHz oscilloscope on a chip), allowing offline analysis of the full pulse shape for sub-10 ps timing. The cost is high power (~1 W per channel) and large data volume, restricting these chips to low-channel-count applications such as TORCH (Section 9.1). EICROC offers also this capability, sampling the waveform in several points.

12. Future Challenges

The path from today’s 25–50 ps systems to the <10 ps required by FCC-hh and FCC-ee is not merely evolutionary; it requires solutions to several fundamental problems.

Low-power timing ASICs. Current 28 nm demonstrators consume ~1.5–2 W/cm², a factor of five above what can be removed by evaporative CO₂ cooling without unacceptable material budget. Achieving <0.5 W/cm² at ~10 ps requires either a radical reduction in power through novel circuit topologies or architectural innovations such as deep resource sharing.

Radiation hardness to 10¹⁶ n_{eq}/cm². Standard LGADs lose their gain layer at fluences above ~2×10¹⁵ n_{eq}/cm². The *Compensated LGAD* concept [43] co-implants donor atoms to partially compensate the acceptor removal, extending the useful gain to fluences approaching 10¹⁶ n_{eq}/cm². Alternatively, 3D trench sensors (which have no gain layer to destroy) can operate at the highest fluences with ~10 ps intrinsic timing, but require more complex fabrication and the temporal resolution degrades rapidly as the pixel size increases above the presently used 50–55 μm.

Picosecond clock distribution. A timing resolution of 10 ps requires distributing a clock with <5 ps jitter across millions of channels. Optical clock distribution schemes, which avoid the impedance mismatches of electrical networks, are under investigation.

| Era | Technology | Resolution | Channels | Integration |
|-----------|---------------------------|------------|-----------------|---------------------|
| 1990–2005 | Scint. + PMT + NIM crates | 100–200 ps | 10^2 – 10^5 | Dedicated subsystem |
| 2005–2025 | SiPM / LGAD + ASIC | 25–80 ps | 10^5 – 10^7 | Timing layer (3+1) |
| 2025–2040 | LGAD / 3D + 28 nm ASIC | 10–30 ps | 10^6 – 10^8 | 4D at every hit |
| 2040+ | Monolithic LGAD | <10 ps | 10^8 – 10^9 | Ubiquitous 4D |

Table 9: The four generations of timing in particle physics.

Thermal management. Even at 0.5 W/cm^2 , a large tracking system of $\mathcal{O}(10) \text{ m}^2$ dissipates $\mathcal{O}(50) \text{ kW}$. Evaporative CO_2 cooling is the current standard, but its mass ($\sim 1\% X_0$ per cooling circuit) competes with the material budget, particularly in inner tracker layers.

13. Conclusions

The history of timing in particle physics is a story of increasing integration: from a PMT behind a scintillator bar, to a dedicated timing layer of silicon pixels, to time as a fourth coordinate measured at every hit in a tracking detector.

Table 9 summarises the four generations in terms of their key performance figures.

The silicon revolution, enabled by SiPM, LGAD, and timing ASICs, transformed timing from a specialised technique into a mainstream detector capability. The systems under construction at the HL-LHC – CMS MTD, ATLAS HGTD, and CMS HGCAL – demonstrate the maturity of this technology at the million-channel scale with 25–50 ps resolution. The EIC, LHCb VELO Upgrade II, and ALICE 3 push into new regimes, with LHCb providing the first example of full 4D tracking in a collider environment. Future facilities, from the FCC-ee precision factory to the extreme environment of the Muon Collider and the enormous pile-up of the FCC-hh, require a further leap to ~ 10 ps, setting a clear and demanding R&D agenda. The dominant challenges are power, radiation hardness, and clock distribution – all solvable in principle, but requiring sustained investment in sensor and ASIC development over the coming decade. The transition from today’s 25–50 ps systems to the <10 ps regime is constrained as much by fundamental fluctuation limits as by engineering ingenuity.

Acknowledgements

The author thanks the many colleagues in the LGAD, SiPM, and timing ASIC communities whose work is reviewed here. This paper was presented at TIPP2026, Mumbai.

References

- [1] D. Acosta et al. (CDF Collaboration), *The CDF time-of-flight detector*, Nucl. Instrum. Meth. A **518** (2004) 605.
- [2] V. Fanti et al. (NA48 Collaboration), *A new measurement of direct CP violation in two pion decays of the neutral kaon*, Phys. Lett. B **465** (1999) 335.
- [3] A. Alavi-Harati et al. (KTeV Collaboration), *Observation of direct CP violation in $K_{S,L} \rightarrow \pi\pi$ decays*, Phys. Rev. Lett. **83** (1999) 22.
- [4] M. Aguilar et al. (AMS Collaboration), *The Alpha Magnetic Spectrometer (AMS) on the International Space Station*, Phys. Rep. **366** (2002) 331.

- [5] Y. Fukuda et al. (Super-Kamiokande Collaboration), *Evidence for an oscillatory signature in atmospheric neutrino oscillation*, Phys. Rev. Lett. **81** (1998) 1562.
- [6] F. Anghinolfi et al., *NINO: an ultra-fast and low-power front-end amplifier-discriminator ASIC designed for the multigap resistive plate chamber*, Nucl. Instrum. Meth. A **533** (2004) 183.
- [7] J. Christiansen, *HPTDC High Performance Time to Digital Converter*, CERN/EP-MIC, v2.2 (2004).
- [8] ALICE Collaboration, *ALICE Time-Of-Flight system (TOF): Technical Design Report*, CERN/LHCC 2000-012 (2000).
- [9] B. Aubert et al. (BaBar Collaboration), *The BaBar detector*, Nucl. Instrum. Meth. A **479** (2002) 1.
- [10] Belle II Collaboration, *The Belle II Physics Book*, PTEP **2019** (2019) 123C01.
- [11] D. Renker and E. Lorenz, *Advances in solid state photon detectors*, JINST **4** (2009) P04004.
- [12] G. Pellegrini et al., *Technology developments and first measurements of Low Gain Avalanche Detectors (LGAD) for high energy physics applications*, Nucl. Instrum. Meth. A **765** (2014) 12.
- [13] N. Cartiglia et al., *Design optimization of Ultra-Fast Silicon Detectors*, Nucl. Instrum. Meth. A **796** (2015) 141.
- [14] H. Sadrozinski, A. Seiden, N. Cartiglia, *4D tracking with ultra-fast silicon detectors*, Rep. Prog. Phys. **81** (2018) 026101.
- [15] M. Moll, *Acceptor removal – Displacement damage effects involving the shallow acceptor doping of p-type silicon devices*, Nucl. Instrum. Meth. A **924** (2019) 97.
- [16] M. Mandurrino et al., *Demonstration of 200-, 100-, and 50- μ m pitch resistive AC-coupled silicon detectors (RSD) with 100% fill factor for 4D particle tracking*, IEEE Electron Device Lett. **40** (2019) 1780.
- [17] G. Aglieri Rinella et al., *The GigaTracker: A sub-100 ps time-stamping silicon pixel detector for the NA62 experiment at CERN*, JINST **14** (2019) P07010.
- [18] I. Neri et al., *The TDCPix ASIC for the NA62 GigaTracker*, JINST **7** (2012) C01001.
- [19] CMS Collaboration, *A MIP timing detector for the CMS Phase-2 upgrade*, CERN/LHCC 2019-003, CMS-TDR-020 (2019).
- [20] G. Cerminara et al., *The TOFHIR2 ASIC for the CMS Barrel Timing Layer*, JINST **17** (2022) C03018.
- [21] CMS Collaboration, *ETROC: the readout ASIC for the CMS ETL*, CMS-DN-21-001 (2021).
- [22] ATLAS Collaboration, *Technical Design Report: A High-Granularity Timing Detector for the ATLAS Phase-II Upgrade*, CERN/LHCC 2020-007, ATL-TDR-31 (2020).
- [23] S. Xie et al., *Design and performance of the Fermilab Constant Fraction Discriminator ASIC*, Nucl. Instrum. Meth. A **1056** (2023) 168655.
- [24] C. Agapopoulou et al., *Performance of a front-end prototype ASIC for the ATLAS High Granularity timing detector*, JINST **18** (2023) P08019.
- [25] CMS Collaboration, *The Phase-2 Upgrade of the CMS Endcap Calorimeter*, CERN/LHCC 2017-023, CMS-TDR-019 (2017).
- [26] PIONEER Collaboration, *PIONEER: Studies of rare pion decays*, arXiv:2203.01981 (2022).
- [27] A. Accardi et al., *Electron-Ion Collider: The Next QCD Frontier*, Eur. Phys. J. A **52** (2016) 268.
- [28] EIC Collaboration, *EICROC: the readout ASIC for EIC AC-LGAD TOF*, ePIC technical note (2023).
- [29] LHCb Collaboration, *LHCb VELO Upgrade II: Expression of Interest*, CERN-LHCC-2022-002 (2022).
- [30] O.A. de Aguiar Francisco, *The LHCb VELO Upgrade II: Design and development of the readout electronics*, Nucl. Instrum. Meth. A **1063** (2024) 169238.
- [31] ALICE Collaboration, *Letter of intent for ALICE 3: A next-generation heavy-ion experiment at the LHC*, arXiv:2211.02491 (2022).
- [32] FCC Collaboration, *FCC-ee: The Lepton Collider*, Eur. Phys. J. Spec. Top. **228** (2019) 261.
- [33] FCC Collaboration, *FCC-hh: The Hadron Collider*, Eur. Phys. J. Spec. Top. **228** (2019) 755.
- [34] C. Aime et al., *Muon Collider Physics Summary*, arXiv:2203.07256 (2022).
- [35] M. Milanesio et al., *TIMESPOT1: A 28-nm CMOS Pixel ASIC for 4D tracking in high-hit rate environments*, JINST **17** (2022) C11004.
- [36] D. Breton et al., *The SAMPIC waveform and time-to-digital converter*, IEEE NSS/MIC (2014).
- [37] E. Diociaiuti et al., *CriLin: A CRystal calorImeter with Longitudinal INformation for future lepton colliders*, arXiv:2204.12232 (2022).
- [38] A. Lucchini et al., *New perspectives on segmented crystal calorimeters for future colliders*, JINST **15** (2020) P11005.
- [39] T. Gys et al., *The TORCH detector: R&D towards a large-scale device*, Nucl. Instrum. Meth. A **952** (2020) 161783.
- [40] J. Bortfeldt et al., *PICOSEC: Charged particle timing at sub-25 picosecond precision with a Cherenkov based Micromegas detector*, Nucl. Instrum. Meth. A **903** (2018) 317.
- [41] R. Bolzonella et al., *Development and characterization of hybrid MCP-PMT with embedded Timepix4 ASIC used as pixelated anode*, Nucl. Instrum. Meth. A **1082** (2026) 170965.
- [42] M. Ferrero et al., *FAST3 ASIC: an analog front-end with 30 ps resolution, designed to readout thin Low Gain Avalanche Diodes*, JINST **20** (2025) C03007.

[43] V. Sola et al., *A compensated design of the LGAD gain layer*, Nucl. Instrum. Meth. A **1041** (2022) 167228.